iScience

CellPress
OPEN ACCESS

Article

JAK inhibitors dampen activation of interferon-activated transcriptomes and the SARS-CoV-2 receptor ACE2 in human renal proximal tubules

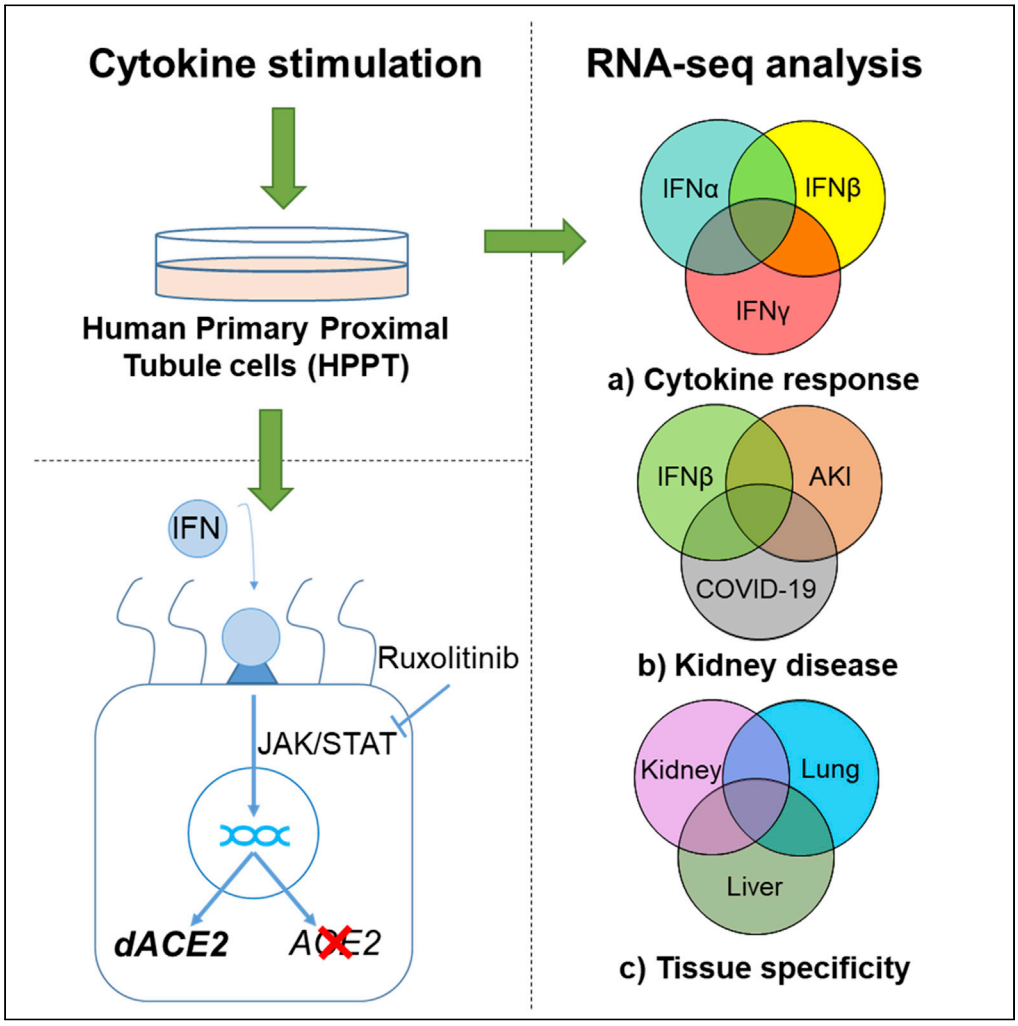

Jakub Jankowski, Hye Kyung Lee, Julia Wilflingseder, Lothar Hennighausen

jakub.jankowski@nih.gov (J.J.)
lotharh@nih.gov (L.H.)

Highlights

We provide transcriptomic and epigenetic data sets for human renal proximal tubules

Cytokine stimulation induces distinct genetic pathways in the kidney

Short isoform of *ACE2*, *dACE2*, is expressed in renal proximal tubules

Type I interferons increase *dACE2*, but not full *ACE2* expression

Jankowski et al., iScience *24*, 102928
August 20, 2021
https://doi.org/10.1016/j.isci.2021.102928

iScience

CellPress
OPEN ACCESS

Article

JAK inhibitors dampen activation of interferon-activated transcriptomes and the SARS-CoV-2 receptor ACE2 in human renal proximal tubules

Jakub Jankowski,[1,2,*] Hye Kyung Lee,[1] Julia Wilflingseder,[2] and Lothar Hennighausen[1,3,*]

SUMMARY

SARS-CoV-2 infections initiate cytokine storms and activate genetic programs leading to progressive hyperinflammation in multiple organs of patients with COVID-19. While it is known that COVID-19 impacts kidney function, leading to increased mortality, cytokine response of renal epithelium has not been studied in detail. Here, we report on the genetic programs activated in human primary proximal tubule (HPPT) cells by interferons and their suppression by ruxolitinib, a Janus kinase (JAK) inhibitor used in COVID-19 treatment. Integration of our data with those from patients with acute kidney injury and COVID-19, as well as other tissues, permitted the identification of kidney-specific interferon responses. Additionally, we investigated the regulation of the recently discovered isoform (dACE2) of the angiotensin-converting enzyme 2 (ACE2), the SARS-CoV-2 receptor. Using ChIP-seq, we identified candidate interferon-activated enhancers controlling the *ACE2* locus, including the intronic *dACE2* promoter. Taken together, our study provides an in-depth understanding of genetic programs activated in kidney cells.

INTRODUCTION

A form of acute respiratory distress syndrome (ARDS) caused by SARS-CoV-2 is a major contributor to the death toll of COVID-19 (Gibson et al., 2020). ARDS is closely linked to cytokine storm, an unrestrained release of proinflammatory cytokines and chemokines (Kim et al., 2021). This, in turn, may result in multi-organ failure (Mokhtari et al., 2020) and coagulopathies (Vinayagam and Sattu, 2020), affecting, amongst others, the kidney (Ahmadian et al., 2021). Acute kidney injury (AKI), potentially resulting from cytokine storm (Chong and Saha, 2021), is a known complication of COVID-19, and it has also been proposed that decline in renal function in hospitalized patients is caused by the virus itself (Lynch and Tang, 2020). Even before the SARS-CoV-2 pandemic, AKI was a significant medical and socioeconomic burden, with estimated one in three intensive care patients suffering from decline in kidney function (Hoste et al., 2018).

In addition to other mechanisms, SARS-CoV-2 was shown to able to infect kidney epithelium, directly contributing to organ damage (Braun et al., 2020; Peng et al., 2020; Su et al., 2020; Sun et al., 2020). It is known that its infectivity depends on the receptor, angiotensin-converting enzyme 2 (ACE2) (Hoffmann et al., 2020). Physiologically, ACE2 serves as an element of renin-angiotensin-aldosterone system and bradykinin system (Donoghue et al., 2000; Tipnis et al., 2000). In SARS-CoV-2 infection, the viral spike protein binds ACE2 and facilitates viral entry into cells. ACE2 expression has been detected in the kidney (Sungnak et al., 2020) and proximal tubules via single-cell transcriptome analysis (Chen et al., 2020; He et al., 2020). However, transcriptional regulation of *ACE2* and its expression pattern in the kidney are poorly understood. Human studies indicate that changes in *ACE2* expression are linked to type 2 diabetic nephropathy (Mizuiri et al., 2008), IgA nephropathy (Mizuiri et al., 2011), hypertension (Koka et al., 2008), and nephrosclerosis (Wang et al., 2010). Usually, decrease in ACE2 is associated with disease, which may dysregulate ACE/ACE2 ratio; however, both ACE and ACE2 may be regulated by independent pathways (Mizuiri and Ohashi, 2015).

Recently, a new isoform of *ACE2*, *deltaACE2* (*dACE2*), was identified in several cell types (Blume et al., 2020; Fignani et al., 2020; Lee et al., 2021; Ng et al., 2020; Onabajo et al., 2020). Contrary to earlier reports (Ziegler et al., 2020), where *ACE2* was suggested to be an interferon-stimulated gene (ISG), its new isoform *dACE2*

[1]Laboratory of Genetics and Physiology, National Institute of Diabetes and Digestive and Kidney Diseases, U.S. National Institutes of Health, Building 8, Room 101, 8 Center Dr, Bethesda, MD 20892, USA

[2]Department of Physiology and Pathophysiology, University of Veterinary Medicine, Veterinärplatz 1, 1210 Vienna, Austria

[3]Lead contact

*Correspondence: jakub.jankowski@nih.gov (J.J.), lotharh@nih.gov (L.H.)

https://doi.org/10.1016/j.isci.2021.102928

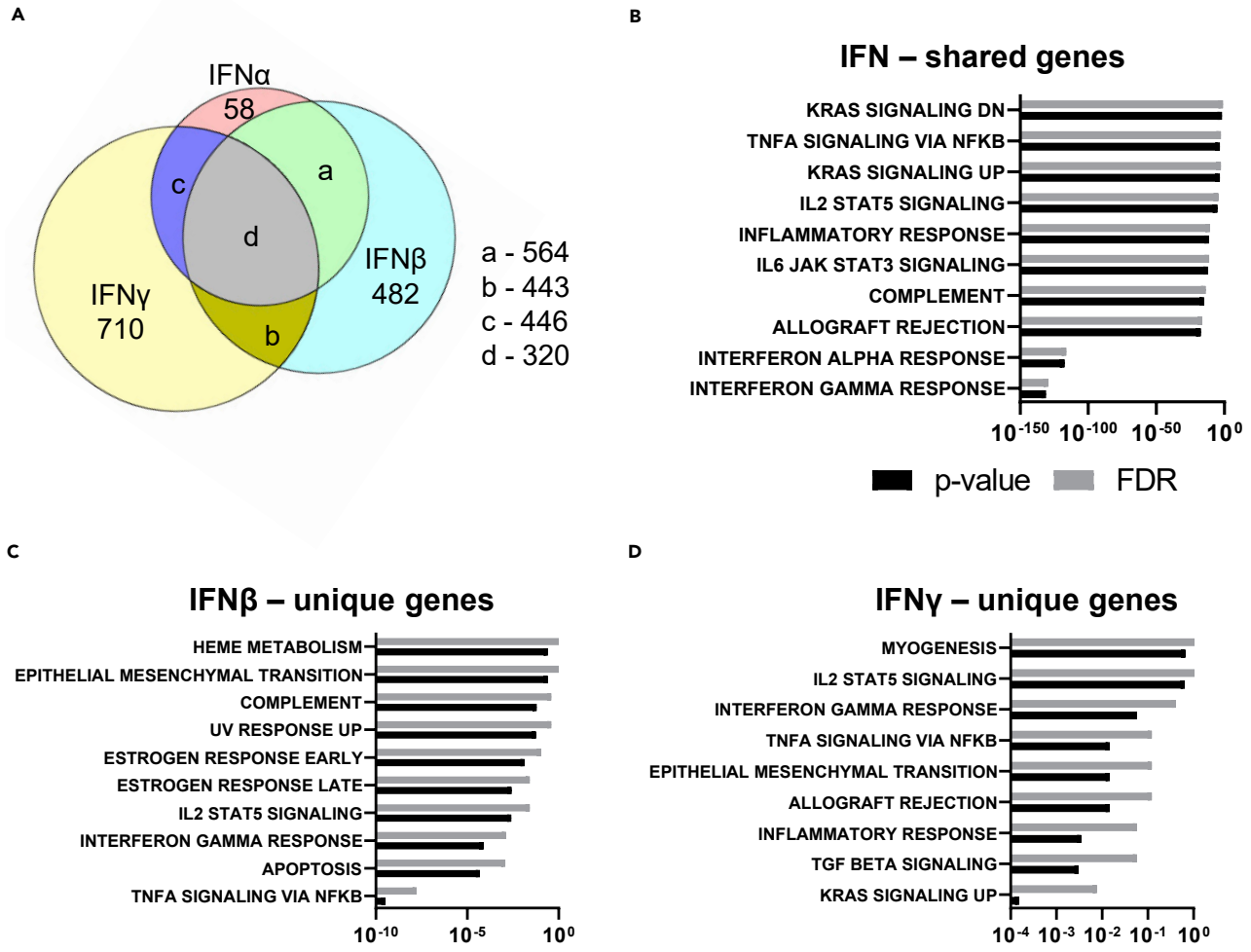

Figure 1. Comparison of signaling pathways induced by IFNα, IFNβ, and IFNγ stimulation of HPPT cells

(A) Venn diagram of unique and common genes induced by each cytokine.

(B–D) GSEA results of p values and FDR in top 10 significantly represented pathways in gene groups shared by all three conditions and unique for IFNβ and IFNγ. See also Tables S1–S3.

expression appears to be significantly regulated by cytokine or viral stimulation. In fact, in some cells, such as pancreatic β-cells, *dACE2* may be the prevalent isoform even at the baseline (Fignani et al., 2020). Usually, decrease in *ACE2* expression is linked with disease progression; however, it is unknown whether *dACE2* has an impact on these readouts, as methods used to this date assessed *ACE2* without discerning between isoforms. Additionally, increased *ACE2* levels were found in several animal models of kidney disease, and contribution of *dACE2* to these changes remains to be assessed (Moon et al., 2008).

Here, for the first time, we show global transcriptional regulation in cytokine-stimulated human primary proximal tubule (HPPT) cells. We assess overlaps between responses to IFNα, IFNβ, and IFNγ, and we compare IFNβ-stimulated genetic programs to available AKI and COVID-19 data sets to investigate shared pathways in renal response to injury. We show interferon-inducible genetic pathways unique for the kidney and shared with other human tissues. We assess interferon stimulated gene downregulation by JAK inhibitor ruxolitinib and, finally, describe in detail the regulatory landscape of the *ACE2* locus in renal proximal tubule cells.

These findings provide in-depth understanding of interferon-mediated immune responses in the kidney, especially in the context of *ACE2* activation observed in SARS-CoV-2 infection, and may serve as a basis for better understanding of the commonalities and differences between cytokine stimulation of various tissues.

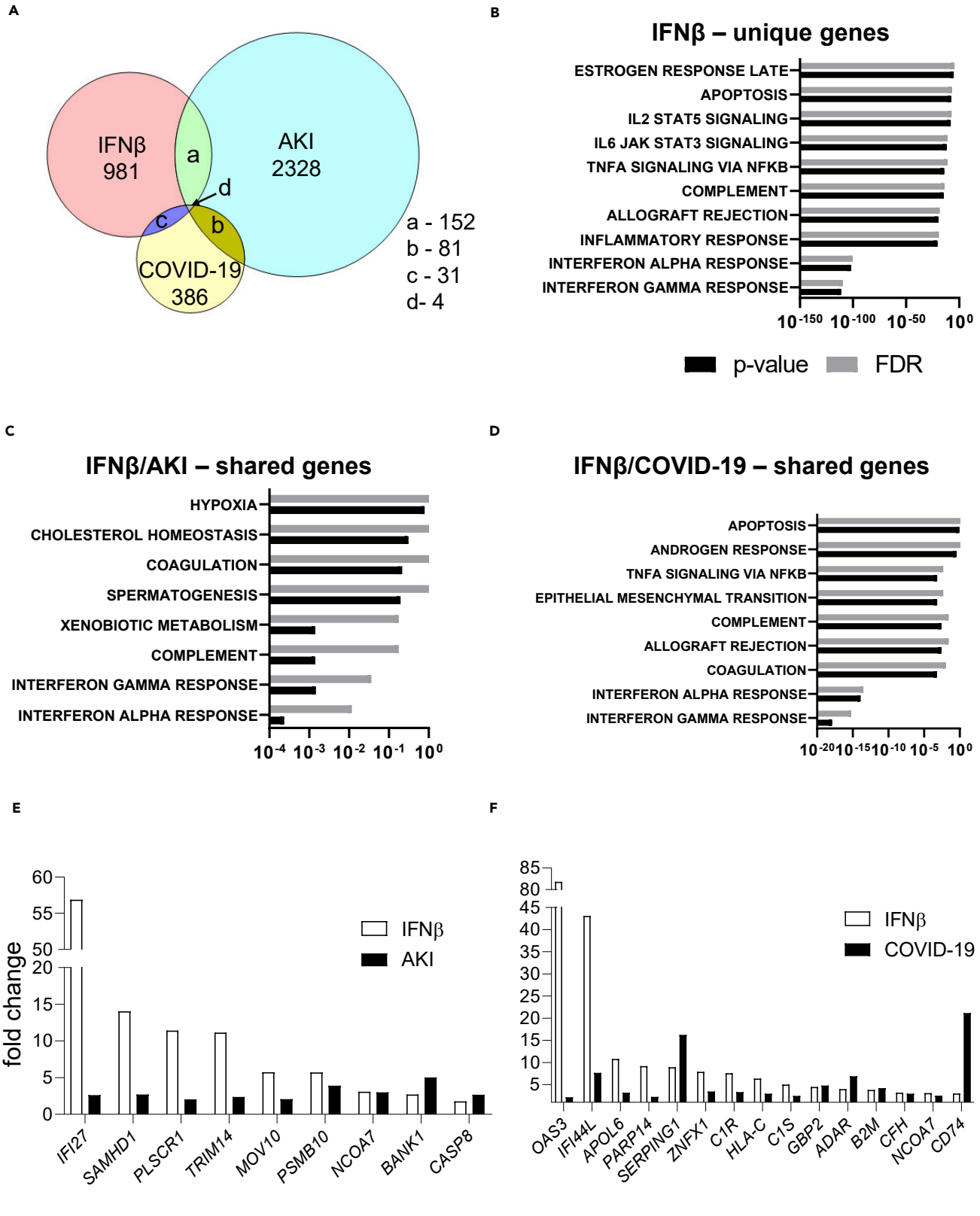
A
IFNβ
981
AKI
2328
COVID-19
386
a
b
c
d
a - 152
b - 81
c - 31
d- 4
B
IFNβ – unique genes
ESTROGEN RESPONSE LATE
APOPTOSIS
IL2 STAT5 SIGNALING
IL6 JAK STAT3 SIGNALING
TNFA SIGNALING VIA NFKB
COMPLEMENT
ALLOGRAFT REJECTION
INFLAMMATORY RESPONSE
INTERFERON ALPHA RESPONSE
INTERFERON GAMMA RESPONSE
10-150 10-100 10-50 100
p-value
FDR
C
IFNβ/AKI – shared genes
HYPOXIA
CHOLESTEROL HOMEOSTASIS
COAGULATION
SPERMATOGENESIS
XENOBIOTIC METABOLISM
COMPLEMENT
INTERFERON GAMMA RESPONSE
INTERFERON ALPHA RESPONSE
10-4 10-3 10-2 10-1 100
D
IFNβ/COVID-19 – shared genes
APOPTOSIS
ANDROGEN RESPONSE
TNFA SIGNALING VIA NFKB
EPITHELIAL MESENCHYMAL TRANSITION
COMPLEMENT
ALLOGRAFT REJECTION
COAGULATION
INTERFERON ALPHA RESPONSE
INTERFERON GAMMA RESPONSE
10-20 10-15 10-10 10-5 100
E
fold change
60
55
50
20
15
10
5
0
IFNβ
AKI
IFI27
SAMHD1
PLSCR1
TRIM14
MOV10
PSMB10
NCOA7
BANK1
CASP8
F
85
80
45
40
35
30
25
20
15
10
5
IFNβ
COVID-19
OAS3
IFI44L
APOL6
PARP14
SERPING1
ZNFX1
C1R
HLA-C
C1S
GBP2
ADAR
B2M
CFH
NCOA7
CD74

Figure 2. Comparison of signaling pathways induced by IFNβ stimulation of HPPT cells, and human kidneys during AKI and COVID-19 infection
(A) Venn diagram of unique and common genes induced by IFNβ, AKI, and COVID-19.
(B–D) GSEA results of p values and FDR in top 10 significantly represented pathways in gene groups unique for HPPT and shared between HPPT and COVID-19 or AKI.
(E and F) Comparison of fold increase in expression of shared genes involved in IFN signaling in HPPT vs AKI and COVID-19 (in relation to untreated, healthy, and mild COVID-19 samples, respectively). See also Tables S1–S3.

RESULTS

To investigate renal cytokine-induced genetic programs, we conducted unbiased RNA-seq analyses on HPPT cells treated for 12 hr with IFNα, IFNβ, IFNγ, or IL-1β. A total of 746 genes were significantly induced by IFNα, 1169 by IFNβ, 1280 by IFNγ, and 2190 by IL-1β (Tables S1 and S2). Next, we investigated the degree of interferon response overlap. IFNα induced expression of 58 unique genes, while IFNβ and IFNγ induced 482 and 710 genes, respectively (Figure 1A). The overlap between all three interferons (320 genes) was enriched for interferon response genes (Figure 1B and Table S3), while gene sets unique for IFNβ and IFNγ were more diverse (Figures 1C and 1D). Next, we focused on IFNβ. It statistically significantly altered the most diverse signaling pathways as identified by Gene Set Enrichment Analysis (GSEA) (Table S3); it is also a known antiviral used against COVID-19. Additionally, several public transcriptomic data sets from cells treated with IFNβ are available to help elucidate interferon-regulated genetic programs specific for renal epithelium.

First, we compared whether expression patterns in patients with AKI (Park et al., 2020) and patients with severe COVID-19 (Desai et al., 2020) bear resemblance to those stimulated in HPPT cells by IFNβ. To our knowledge, only one RNA-seq data set with human ischemia-reperfusion AKI data is publicly available (Park et al., 2020). Similarly, only one renal data set from patients with COVID-19 could be found for our comparison, differentiating between severe and nonsevere disease (Desai et al., 2020). IFNβ stimulation of HPPT cells resulted in upregulation of 981 unique genes compared with other conditions (Figures 2A and 2B). AKI resulted in increased expression of 2566 genes including 156 shared with IFNβ-stimulated HPPT cells (Figures 2A and 2C; Table S3). Expression of 35 genes was induced in both severe COVID-19 and IFNβ-treated HPPT cells (Figures 2A and 2D; Table S3). Although more genes were shared between IFNβ-HTTP and AKI than between IFNβ-HPPT and COVID-19, genes involved in the interferon signaling pathways were preferentially activated in IFNβ-HPPT cells and COVID-19 compared to IFNβ-HPPT cells and AKI (Figures 2C and 2D). We also visualized the genes identified as involved in interferon signaling pathway and overlapping between conditions to see whether similar fold increases in expression can be observed (Figures 2E and 2F). The degree of gene induction varied between data sets, possibly reflecting differences in sample type and technical preparation.

Next, to elucidate cell-specific and common genes induced by IFNβ in primary cells and cell lines, we compared our HPPT data (12-hr *in vitro* IFNβ treatment) with similarly treated human primary lung epithelium (Lee et al., 2021) and the PH5CH8 hepatocyte cell line (Forero et al., 2019) (Figure 3). A total of 685 genes were uniquely activated in HPPT cells, 203 in the lung cells, and 198 in the liver, showing tissue-specific gene induction by cytokine stimulation (Figures 3A and 3B). IFNβ-stimulated renal cells shared 444 genes with the lung and 195 with the liver, and 154 genes were common for all three tissues. They are enriched in various immune hallmarks in GSEA analysis (Figures 3C and 3D), and average fold read increase of genes most upregulated in HPPT cells did not correlate with other tissues (Figures 3E and 3F).

To gauge the extent of IFNβ response through the JAK/STAT pathway, we compared gene expression of cells stimulated by IFNβ to cells cultured additionally with the JAK inhibitor ruxolitinib (Figure 4, Table S3). Immune response genes were significantly enriched in the gene set upregulated by IFNβ, and their expression was dampened by ruxolitinib in RNA-seq analysis. We identified interleukins (*IL4I1, IL15*), toll-like receptors (*TLR2, TLR4*), interferon regulatory factors (*IRF1, IRF7, IRF9*), interferon-induced proteins (*IFIT1, IFIT2, IFIT3, IFI44*), and chemoattractants (*CXCL10, CXCL11*) as significantly upregulated by type I interferons (Figure 4, Table S2). Extended GSEA analyses for all data presented here can be found in Table S3.

Recent research (Blume et al., 2020; Lee et al., 2021; Ng et al., 2020; Onabajo et al., 2020) revealed the presence of an alternative promoter expressing *deltaACE2* (*dACE2*), a short isoform of *ACE2*, within intron 9 of the *ACE2* gene. Although some studies found the presence of *dACE2* RNA in healthy kidney tissue and tumors (Ng et al., 2020; Onabajo et al., 2020), its structure, function, and the presence of regulatory

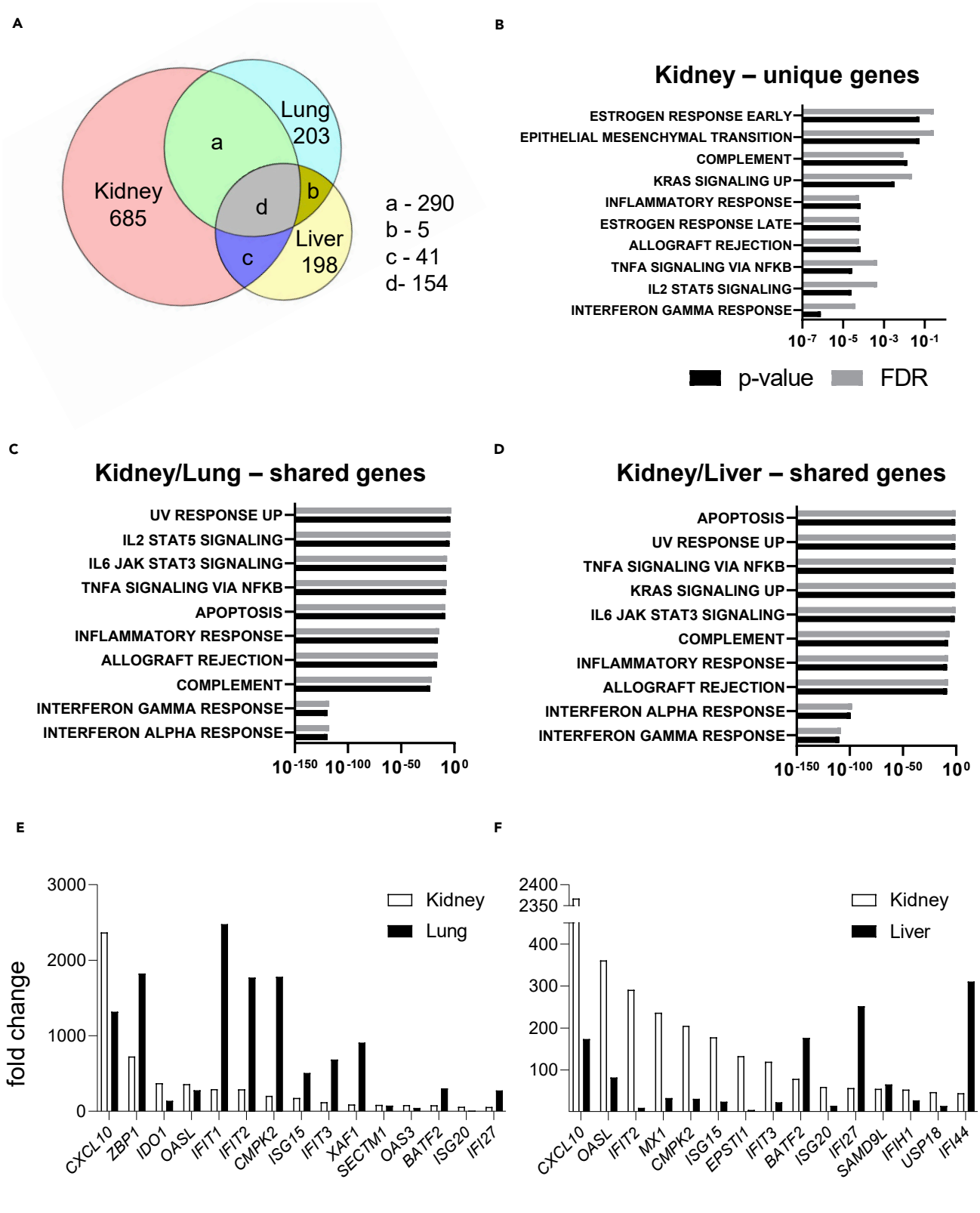
A
Kidney
685
Lung
203
Liver
198
a
b
c
d
a - 290
b - 5
c - 41
d- 154
B
Kidney – unique genes
ESTROGEN RESPONSE EARLY
EPITHELIAL MESENCHYMAL TRANSITION
COMPLEMENT
KRAS SIGNALING UP
INFLAMMATORY RESPONSE
ESTROGEN RESPONSE LATE
ALLOGRAFT REJECTION
TNFA SIGNALING VIA NFKB
IL2 STAT5 SIGNALING
INTERFERON GAMMA RESPONSE
10-7 10-5 10-3 10-1
p-value
FDR
C
Kidney/Lung – shared genes
UV RESPONSE UP
IL2 STAT5 SIGNALING
IL6 JAK STAT3 SIGNALING
TNFA SIGNALING VIA NFKB
APOPTOSIS
INFLAMMATORY RESPONSE
ALLOGRAFT REJECTION
COMPLEMENT
INTERFERON GAMMA RESPONSE
INTERFERON ALPHA RESPONSE
10-150 10-100 10-50 100
D
Kidney/Liver – shared genes
APOPTOSIS
UV RESPONSE UP
TNFA SIGNALING VIA NFKB
KRAS SIGNALING UP
IL6 JAK STAT3 SIGNALING
COMPLEMENT
INFLAMMATORY RESPONSE
ALLOGRAFT REJECTION
INTERFERON ALPHA RESPONSE
INTERFERON GAMMA RESPONSE
10-150 10-100 10-50 100
E
fold change
3000
2000
1000
0
Kidney
Lung
CXCL10 ZBP1 IDO1 OASL IFIT1 IFIT2 CMPK2 ISG15 IFIT3 XAF1 SECTM1 OAS3 BATF2 ISG20 IFI27
F
2400
2350
400
300
200
100
Kidney
Liver
CXCL10 OASL IFIT2 MX1 CMPK2 ISG15 EPSTI1 IFIT3 BATF2 ISG20 IFI27 SAMD9L IFIH1 USP18 IFI44

Figure 3. Comparison of signaling pathways induced by IFNβ stimulation of HPPT, lung, and liver epithelial cells

(A) Venn diagram of unique and common genes induced by IFNβ in the kidney, lung, or liver epithelial cells.

(B–D) GSEA results of p values and FDR in top 10 significantly represented pathways in gene groups unique for HPPT and shared between HPPT and the lung or liver.

(E and F) Comparison of fold increase in expression of top 15 genes involved in IFN signaling in HPPT vs lung and liver tissue (in relation to untreated cells). See also Tables S1–S3.

elements, as well as cytokine inducibility in kidney cells, have not been investigated. First, we assessed the levels of *ACE2* and *dACE2* mRNA after cytokine treatment using quantitative real-time polymerase chain reaction (qRT-PCR) (Figure 5 and S1). We analyzed the expression of total *ACE2*, serine protease *TMPRSS2* (which primes viral S protein), and the transcription factor *STAT1* to investigate JAK/STAT pathway activation (Figures 5A–5C and S1). While *ACE2* mRNA was increased 6- and 13-fold by IFNα and IFNβ, respectively, expression of the serine protease *TMPRSS2* was not affected by them, but rather was elevated by IL-1β, indicating its regulation by an independent pathway. Expression of *STAT1* was strongly upregulated after interferon treatment. To examine the expression changes of full-length *ACE2* (*flACE2*) and *dACE2* by IFNs, we performed qRT-PCR with isoform-specific primers (Figures 5D and 5E). While *flACE2* was elevated 3-fold, a 300-, 590-, and 27-fold upregulation of *dACE2* was detected upon IFNα, IFNβ, and IFNγ treatments, respectively. Similar increase in gene expression was observed in the studies cited earlier (Table S4).

To investigate whether *flACE2* and *dACE2* are regulated through the JAK/STAT pathway by interferon signaling, we used the JAK inhibitor ruxolitinib (Figures 5F, 5G, and S1). *dACE2* and *STAT1* levels elevated by IFNβ were ablated by ruxolitinib treatment, while no significant changes to full-length *ACE2* expression were observed.

To understand the regulation of the *ACE2* locus by IFNβ and to identify putative genetic control elements of *dACE2* in HPPT cells, we conducted ChIP-seq (Figures 6A–6E) for H3K27ac (active chromatin), H3K4me1 (enhancers), H3K4me3 (promoter marks), and RNA polymerase II loading (Pol II), as well as used available DNase hypersensitive sites (DHS) data set (Thurman et al., 2012).

Candidate regulatory elements were identified at upstream and intronic regions of the *ACE2* locus (Figures 6A–6C). H3K27ac marks and Pol II loading were enriched in the alternative exon 1c in intron 9, the first coding exon of *dACE2*. An increase in RNA-seq reads was detected after treatment, supporting the potential for the presence of a regulatory element (Figures 6C, 6F, and S2). In contrast, full-length *ACE2* promoter marks, which seem to be more pronounced in the kidney than in the lung (Lee et al., 2021), were reduced by IFNβ stimulation. The *STAT1* locus served as a control for the ChIP-seq and after interferon treatment increased H3K4me3 promoter marks and polymerase II binding can be seen, reflecting gene activation (Figure 6D). To confirm the presence of *dACE2*, we amplified and sequenced the novel *dACE2* transcript and confirmed that exon 1c is spliced to exon 10 of *ACE2* (Ng et al., 2020; Onabajo et al., 2020) (Figure S2A). Two TATA-box-like sequences were identified, suggesting the presence of more than one transcription start site (TSS) associated with the intronic promoter (Figure S2B). Additionally, strong H3K27ac marks induced by IFNβ were detected around exon 11 of *ACE2*. These marks are less pronounced in lung cells (Lee et al., 2021). In turn, two putative enhancer elements reported at the site corresponding to 3′ end of *ACE2* gene in lung cells seem to be weaker in the kidney. RNA-seq analyses demonstrated 5-fold IFN-β-induced expression of exon 1c, compared with exon 1a, which harbors the first methionine of the full-length *ACE2* (Figures 6F and S2C). Finally, in addition to the *ACE2* and *TMEM27* promoters, a candidate enhancer element can be seen between the two genes, as indicated by H3K4me1 marks. Additionally, an analysis of the extended *ACE2* locus revealed that *ACE2* and *TMEM27* are under similar interferon regulation and are bordered by CTCF chromatin boundaries, suggesting that they are part of a regulatory unit (Figure S3). The *TMEM27* locus displayed increased H3K27ac and H3K4me3 promoter marks, indicating gene activation after IFNβ treatment (Figure 6E).

DISCUSSION

Our study presents a broad overview of genetic programs stimulated by interferons in renal proximal tubules and compares them with other transcriptomic data. We show robust cytokine response with 1169 genes significantly induced by IFNβ and efficient quenching of gene expression by JAK inhibitor ruxolitinib. Some of those genes are known regulators of renal injury, belonging to divergent pathways, either driving inflammation similar to IRF1 or TLR4 (Wang et al., 2009; Wu et al., 2007) or attenuating it similar to IL4 and IL15 signaling

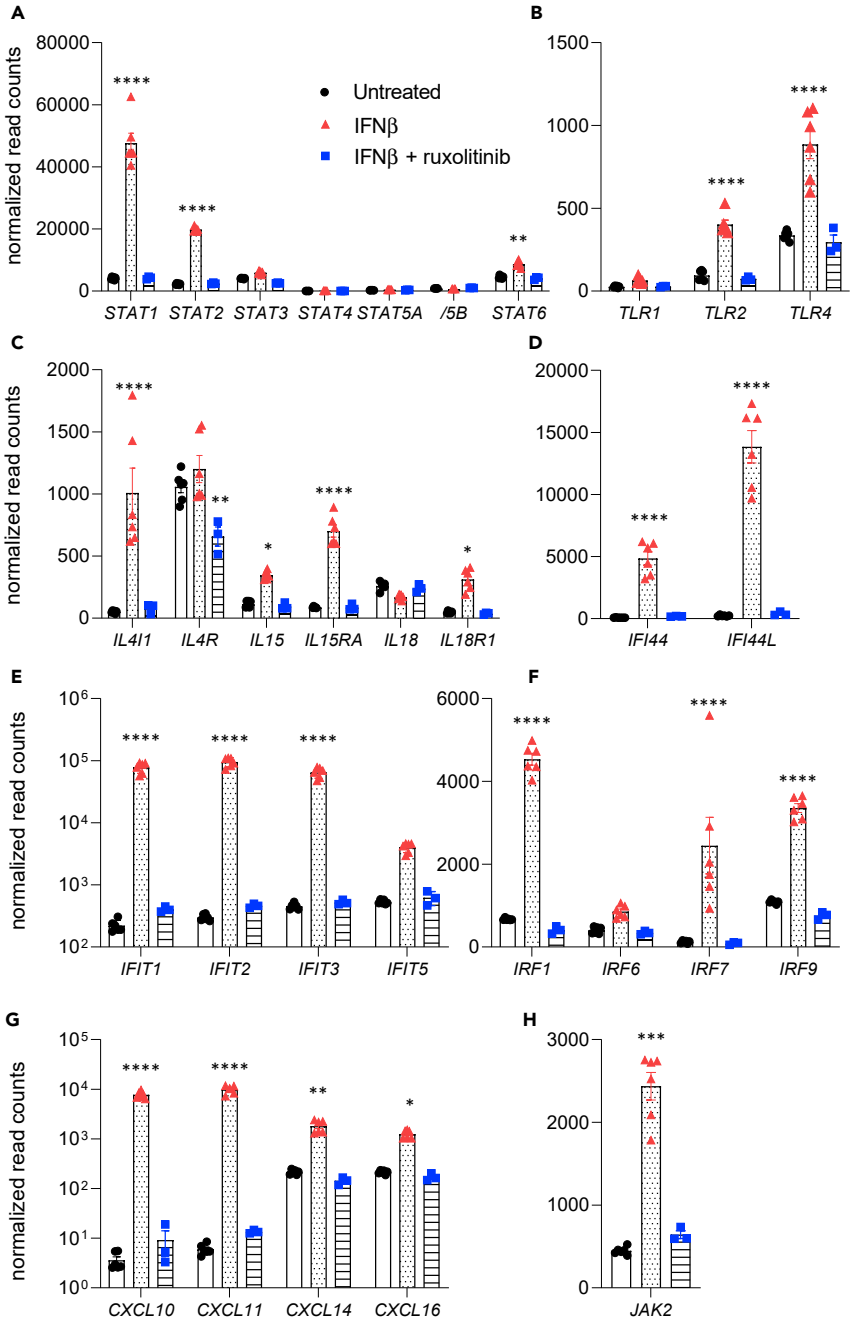

Figure 4. IFNβ-induced immune response genes and their downregulation by ruxolitinib

(A–H) Relative mRNA expression levels of multiple immune genes: (A) STAT gene family, (B) Toll-like receptors, (C) interleukins, (D and E) interferon-induced genes, (F) interferon-regulated factors, (G) CXCL chemokine family, and (H) Janus kinase 2 measured by RNA-seq. Individual data points as well as mean ± SEM of independent biological replicates (n = 3–6) are shown. Significance was analyzed with one-way ANOVA followed by Tukey's multiple comparisons test. *p < 0.05, **p < 0.01, ***p < 0.001, ****p < 0.0001. See also Tables S1–S3.

(Eini et al., 2010; Zhang et al., 2017). There is evidence that type I interferons may contribute to renal damage after ischemic AKI, suggesting that common pathways between IFNβ-treated HPPT cells and AKI could be found (Freitas et al., 2011). Conversely, we expected only a small overlap with SARS-CoV-2-induced genes, as IFNβ has antiviral activity. While we indeed found that interferon stimulation and AKI shared more upregulated genes, interferon-treated cells and COVID-19 samples shared more genes identified as interferon signaling related

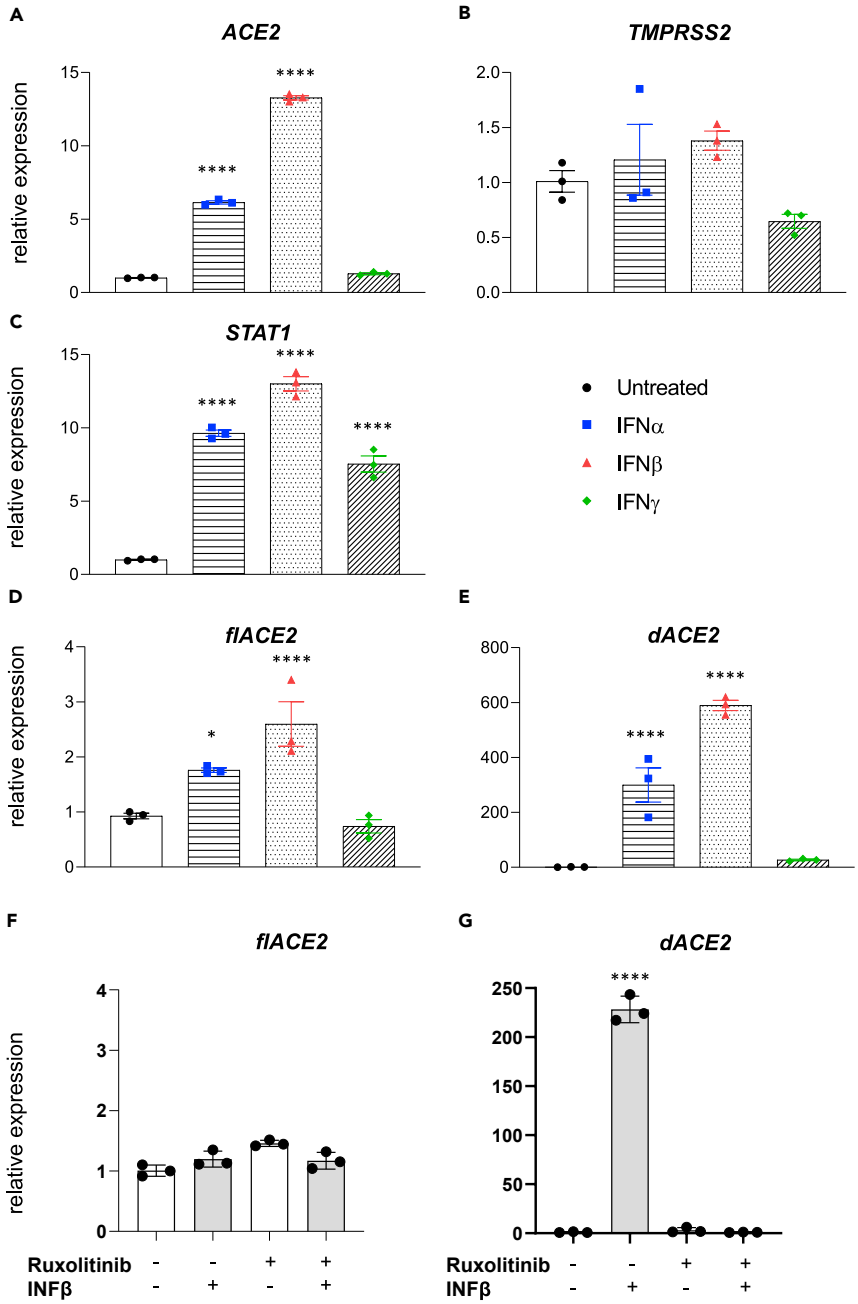

Figure 5. Differences in induction of total ACE2, full-length ACE2, and dACE2 after cytokine treatment

(A) *ACE2*, *TMPRSS2*, and *STAT1* mRNA levels from control and experimental cells were measured by qRT-PCR and normalized to *GAPDH* levels. Relative mRNA levels of (D) full-length *ACE2* (*flACE2*), (E) *dACE2*, after cytokine treatment. (F) *flACE2*, (G) *dACE2* in cells treated with JAK inhibitor ruxolitinib or vehicle, alone or together with IFNβ. Individual data points as well as mean ± SEM of independent biological replicates ($n = 3$) are shown. One- or two-way ANOVA followed by Tukey's multiple comparisons test were used to evaluate the statistical significance of differences relative to untreated cells. ****$p < 0.0001$. See also Figures S1 and S2.

by GSEA analysis. This may not reflect overall trend owing to diversity of AKI and only suggest the degree of similarity with ischemia-reperfusion. We also show uniqueness of renal response when compared with the lung and liver, with over half of the genes upregulated in the kidney being tissue specific. We did not observe significant regulation of *TMPRSS2*, protease involved in SARS-CoV-2 infection, by interferons. Instead, we saw upregulation of *TMPRSS2* expression after IL-1β treatment. Both *IL-1β* and *TMPRSS2* were reported to be

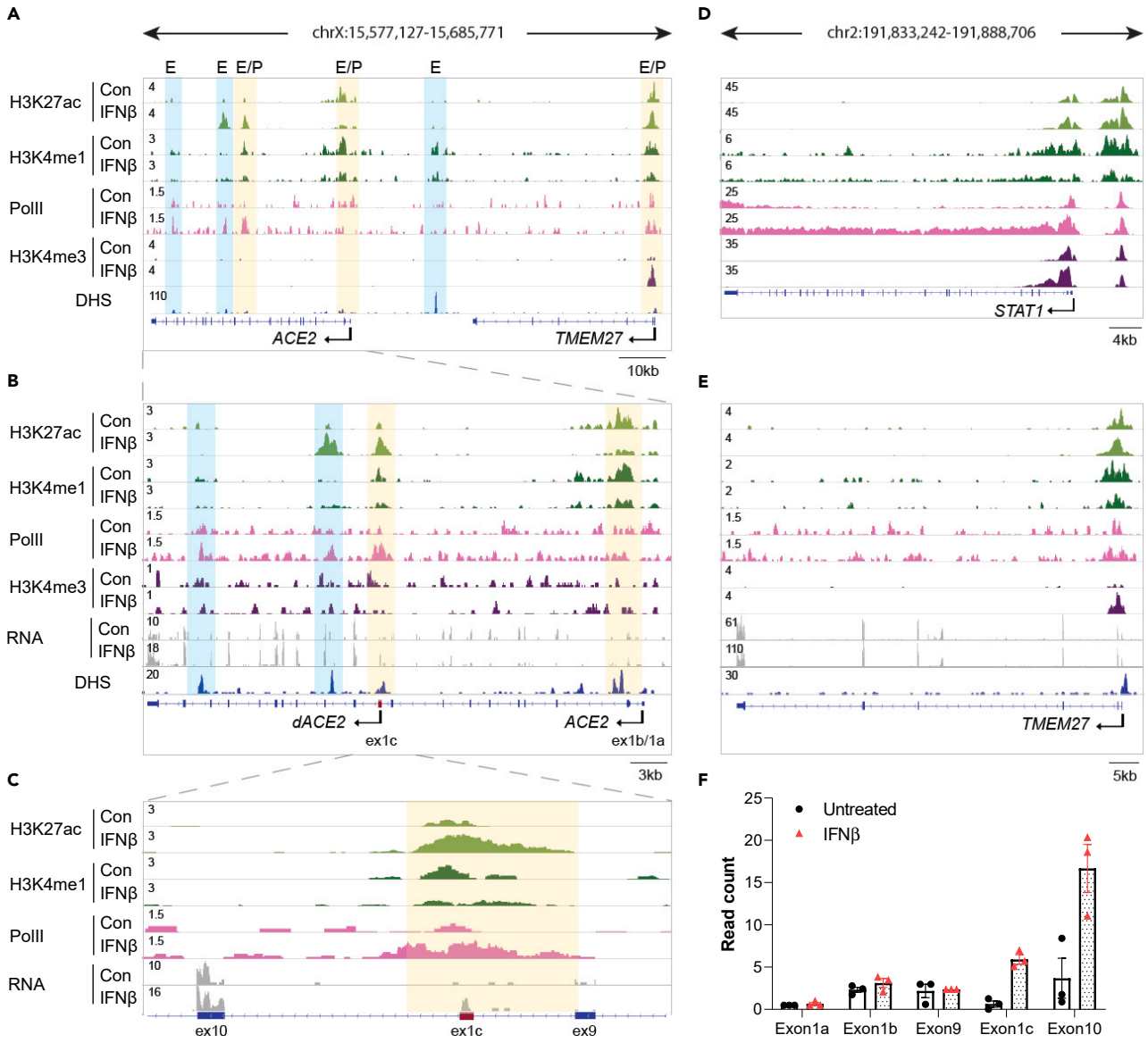

Figure 6. Activation of the novel intronic *ACE2* promoter by IFNβ

(A–E) ChIP-seq data for Pol II and histone markers H3K27ac, H3K4me1, and H3K4me3, DNase hypersensitivity sites and RNA-seq reads at the *ACE2*, *TMEM27*, and *STAT1* locus in human primary proximal tubule (HTTP) cells with and without IFNβ. Solid arrows indicate the orientation of genes. The blue and orange shades indicate regulatory elements, labeled as putative enhancers (E) or promoters (P), respectively.

(F) Number of RNA-seq reads at the exons 1a and 1b, and the new exon 1c. HTTP cells were grown in the absence or the presence of IFNβ. Individual data points as well as mean ± SEM of independent biological replicates (n = 3) are shown. See also Figure S3.

downregulated in nasal basal epithelium after azithromycin treatment (Renteria et al., 2020), reinforcing potential for the link between them. Our study of *ACE2* locus revealed coregulation of *ACE2* and *TMEM27*, which may have additional significance for the kidney, as *TMEM27* gene encodes collectrin, ACE2 homolog, primarily expressed in renal proximal tubule, and collecting duct (Mount, 2007). Collectrin, similarly to ACE2, regulates blood pressure (Chu and Le, 2014) and amino acid transport (Malakauskas et al., 2007). Overall, those results may serve as an important stepping-stone toward further elucidation of kidney-specific genetic programs.

Although our study demonstrates that *dACE2* expression is activated by interferon treatment, further work is needed to identify whether viral infection enhances *dACE2* expression in the kidney. Although several studies have identified *dACE2* after SARS-CoV-2 infection *in vitro*, its biological role remains

unknown. Based on lung epithelium cell data, it is proposed that its extracellular enzymatic and viral spike protein-binding domains are truncated, resulting in partial loss of its carboxypeptidase function. The *dACE2* promoter may be a remnant of a retroviral ISG (Ng et al., 2020). Blume (Blume et al., 2020) reports lack of increase of *ACE2* or *dACE2* after SARS-CoV-2 stimulated BCi-NS1.1 lung cells. Onabajo (Onabajo et al., 2020) similarly shows lack of their upregulation in lung Calu3 cell line, but colon cancer Caco-2 and T84 lines exhibited slightly increased *dACE2* expression after SARS-CoV-2 exposure. This may in part be due to tissue-specific cytokine regulation of *ACE2* and *dACE2*. A standardized and validated detection method of both ACE2 isoforms, as well as understanding of regulatory elements present in *ACE2* locus, is necessary to forward this topic. This is especially true for studies at the protein level, as detection methods such as Western blot are contradictory between reports (Blume et al., 2020; Ng et al., 2020). In our attempts to investigate protein levels of dACE2 using Western blot, we were able to observe a 50-kDa band; however, its presence and intensity were not consistent between various anti-ACE2 antibodies (data not shown). We summarized current knowledge on factors causing dACE2 upregulation in Table S4.

In our study, we present an in-depth analysis and comparison of interferon-stimulated human proximal tubule cells and other experimental data sets, providing insight into genetic pathways driving response to stimuli affecting renal health. In addition, by comparing our data sets with other similarly treated cells, we show unique renal regulation of interferon response. We also identified several putative regulatory elements controlling *ACE2*, as well as confirmed the presence of *dACE2* in renal epithelium. We describe reliance of *dACE2* expression on the JAK/STAT pathway, which may be of clinical importance, as JAK inhibitors are currently used to treat COVID-19 (Cao et al., 2020). Our study strengthens current knowledge about cytokine signaling in renal epithelium, and we believe that it can become a basis for further transcriptomic studies reaching beyond the current efforts to thwart and understand the COVID-19 pandemic.

Limitations of the study

There are several limitations to our study. First, the availability of only a single public RNA-seq data set from patients with AKI is a clear limitation, as AKI is an extremely diverse condition. Additionally, there are no large-scale renal COVID-19 transcriptomics data. Second, reliance on a single batch of primary cells may introduce bias. Third, in an *in vivo* setting, JAK inhibitors have a broader effect than inhibition of genes induced by IFNβ and may affect other cytokines and genetic programs. Finally, the belief in direct SARS-CoV-2 infection of the kidney is not universal despite published evidence.

STAR★METHODS

Detailed methods are provided in the online version of this paper and include the following:

- KEY RESOURCES TABLE
- RESOURCE AVAILABILITY
  - Lead contact
  - Materials availability
  - Data and code availability
- EXPERIMENTAL MODEL AND SUBJECT DETAILS
  - Cell culture
- METHOD DETAILS
  - Cytokine stimulation
  - RNA isolation and qRT-PCR
  - PCR amplification
  - RNA-seq library preparation and data analysis
  - ChIP-seq library preparation and data analysis
- QUANTIFICATION AND STATISTICAL ANALYSIS

SUPPLEMENTAL INFORMATION

Supplemental information can be found online at https://doi.org/10.1016/j.isci.2021.102928.

ACKNOWLEDGMENTS

We thank Ilhan Akan, Sijung Yun, and Harold Smith from the NIDDK genomics core for NGS. Cytokines were gifted by Dr. Marc Ferrer and Olive Jung (NIH/NCATS). This work utilized the computational resources of the NIH HPC Biowulf cluster (http://hpc.nih.gov). This work was supported by the Intramural Research Program (IRP) of the National Institute of Diabetes and Digestive and Kidney Diseases (NIDDK), the NIH Graduate Partnership Program (GPP), and the Austrian Science Fund (P30373).

AUTHOR CONTRIBUTIONS

Conceptualization and methodology: J.J., H.K.L., J.W., and L.H.; Formal analysis and validation, data curation, and visualization: J.J. and H.K.L.; Investigation: J.J.; Resources: L.H.; Writing – original draft: J.J. and H.K.L.; Writing – review and editing: J.J., H.K.L., J.W., and L.H.; Supervision, administration, and funding acquisition: J.W. and L.H. All authors approved the final version of the manuscript.

DECLARATION OF INTERESTS

The authors declare no competing interests.

Received: January 28, 2021
Revised: June 2, 2021
Accepted: July 23, 2021
Published: August 20, 2021

REFERENCES

Ahmadian, E., Hosseiniyan Khatibi, S.M., Razi Soofiyani, S., Abediazar, S., Shoja, M.M., Ardalan, M., and Zununi Vahed, S. (2021). Covid-19 and kidney injury: Pathophysiology and molecular mechanisms. Rev. Med. Virol. *31*, e2176.

Anders, S., Pyl, P.T., and Huber, W. (2015). HTSeq–a Python framework to work with high-throughput sequencing data. Bioinformatics *31*, 166–169.

Blume, C., Jackson, C.L., Spalluto, C.M., Legebeke, J., Nazlamova, L., Conforti, F., Perotin-Collard, J.-M., Frank, M., Crispin, M., Coles, J., et al. (2020). A novel isoform of ACE2 is expressed in human nasal and bronchial respiratory epithelia and is upregulated in response to RNA respiratory virus infection. bioRxiv, 2020.2007.2031.230870.

Bolger, A.M., Lohse, M., and Usadel, B. (2014). Trimmomatic: a flexible trimmer for Illumina sequence data. Bioinformatics *30*, 2114–2120.

Braun, F., Lutgehetmann, M., Pfefferle, S., Wong, M.N., Carsten, A., Lindenmeyer, M.T., Norz, D., Heinrich, F., Meissner, K., Wichmann, D., et al. (2020). SARS-CoV-2 renal tropism associates with acute kidney injury. Lancet *396*, 597–598.

Cao, Y., Wei, J., Zou, L., Jiang, T., Wang, G., Chen, L., Huang, L., Meng, F., Huang, L., Wang, N., et al. (2020). Ruxolitinib in treatment of severe coronavirus disease 2019 (COVID-19): a multicenter, single-blind, randomized controlled trial. J. Allergy Clin. Immunol. *146*, 137–146 e133.

Chen, Q.L., Li, J.Q., Xiang, Z.D., Lang, Y., Guo, G.J., and Liu, Z.H. (2020). Localization of cell receptor-related genes of SARS-CoV-2 in the kidney through single-cell transcriptome analysis. Kidney Dis. (Basel, Switzerland) *6*, 258–270.

Chong, W.H., and Saha, B.K. (2021). Relationship between severe acute respiratory syndrome coronavirus 2 (SARS-CoV-2) and the etiology of acute kidney injury (AKI). Am. J. Med. Sci. *361*, 287–296.

Chu, P., and Le, T. (2014). Role of collectrin, an ACE2 homologue, in blood pressure homeostasis. Curr. Hypertens. Rep. *16*, 490.

Desai, N., Neyaz, A., Szabolcs, A., Shih, A.R., Chen, J.H., Thapar, V., Nieman, L.T., Solovyov, A., Mehta, A., Lieb, D.J., et al. (2020). Temporal and spatial heterogeneity of host response to SARS-CoV-2 pulmonary infection. Nat. Commun. *11*, 6319.

Dobin, A., Davis, C.A., Schlesinger, F., Drenkow, J., Zaleski, C., Jha, S., Batut, P., Chaisson, M., and Gingeras, T.R. (2013). STAR: ultrafast universal RNA-seq aligner. Bioinformatics *29*, 15–21.

Donoghue, M., Hsieh, F., Baronas, E., Godbout, K., Gosselin, M., Stagliano, N., Donovan, M., Woolf, B., Robison, K., Jeyaseelan, R., et al. (2000). A novel angiotensin-converting enzyme-related carboxypeptidase (ACE2) converts angiotensin I to angiotensin 1-9. Circ. Res. *87*, E1–E9.

Eini, H., Tejman-Yarden, N., Lewis, E., Chaimovitz, C., Zlotnik, M., and Douvdevani, A. (2010). Association between renal injury and reduced interleukin-15 and interleukin-15 receptor levels in acute kidney injury. J. Interferon. Cytokine. Res. *30*, 1–8.

Fignani, D., Licata, G., Brusco, N., Nigi, L., Grieco, G.E., Marselli, L., Overbergh, L., Gysemans, C., Colli, M.L., Marchetti, P., et al. (2020). SARS-CoV-2 receptor Angiotensin I-Converting Enzyme type 2 (ACE2) is expressed in human pancreatic β-cells and in the human pancreas microvasculature. bioRxiv, 2020.2007.2023.208041.

Forero, A., Ozarkar, S., Li, H., Chia Heng, L., Hemann, E., Nadjsombati, M., Hendricks, M., So, L., Green, R., Roy, C., et al. (2019). Differential activation of the transcription factor IRF1 underlies the distinct immune responses elicited by type I and type III interferons. Immunity *51*, 451–464.

Freitas, M.C., Uchida, Y., Lassman, C., Danovitch, G.M., Busuttil, R.W., and Kupiec-Weglinski, J.W. (2011). Type I interferon pathway mediates renal ischemia/reperfusion injury. Transplantation *92*, 131–138.

Gibson, P.G., Qin, L., and Puah, S.H. (2020). COVID-19 acute respiratory distress syndrome (ARDS): clinical features and differences from typical pre-COVID-19 ARDS. Med. J. Aust. *213*, 54–56 e51.

He, Q., Mok, T.N., Yun, L., He, C., Li, J., and Pan, J. (2020). Single-cell RNA sequencing analysis of human kidney reveals the presence of ACE2 receptor: a potential pathway of COVID-19 infection. Mol. Genet. Genomic Med. e1442.

Heinz, S., Benner, C., Spann, N., Bertolino, E., Lin, Y.C., Laslo, P., Cheng, J.X., Murre, C., Singh, H., and Glass, C.K. (2010). Simple combinations of lineage-determining transcription factors prime cis-regulatory elements required for macrophage and B cell identities. Mol. Cell *38*, 576–589.

Hoffmann, M., Kleine-Weber, H., Schroeder, S., Kruger, N., Herrler, T., Erichsen, S., Schiergens, T.S., Herrler, G., Wu, N.H., Nitsche, A., et al. (2020). SARS-CoV-2 cell entry depends on ACE2 and TMPRSS2 and is blocked by a clinically proven protease inhibitor. Cell *181*, 271–280.e8.

Hoste, E.A.J., Kellum, J.A., Selby, N.M., Zarbock, A., Palevsky, P.M., Bagshaw, S.M., Goldstein, S.L., Cerda, J., and Chawla, L.S. (2018). Global epidemiology and outcomes of acute kidney injury. Nat. Rev. Nephrol. *14*, 607–625.

Huber, W., Carey, V.J., Gentleman, R., Anders, S., Carlson, M., Carvalho, B.S., Bravo, H.C., Davis, S., Gatto, L., Girke, T., et al. (2015). Orchestrating high-throughput genomic analysis with Bioconductor. Nat. Methods *12*, 115–121.

Kim, J.S., Lee, J.Y., Yang, J.W., Lee, K.H., Effenberger, M., Szpirt, W., Kronbichler, A., and Shin, J.I. (2021). Immunopathogenesis and treatment of cytokine storm in COVID-19. Theranostics *11*, 316–329.

Koka, V., Huang, X.R., Chung, A.C., Wang, W., Truong, L.D., and Lan, H.Y. (2008). Angiotensin II up-regulates angiotensin I-converting enzyme (ACE), but down-regulates ACE2 via the AT1-ERK/p38 MAP kinase pathway. Am. J. Pathol. *172*, 1174–1183.

Langmead, B., Trapnell, C., Pop, M., and Salzberg, S.L. (2009). Ultrafast and memory-efficient alignment of short DNA sequences to the human genome. Genome Biol. *10*, R25.

Lee, H.K., Jung, O., and Hennighausen, L. (2021). JAK inhibitors dampen activation of interferon-stimulated transcription of ACE2 isoforms in human airway epithelial cells. Commun. Biol. *4*, 654.

Lee, J.W., Chou, C.L., and Knepper, M.A. (2015). Deep sequencing in microdissected renal tubules identifies nephron segment-specific transcriptomes. J. Am. Soc. Nephrol. *26*, 2669–2677.

Li, H., Handsaker, B., Wysoker, A., Fennell, T., Ruan, J., Homer, N., Marth, G., Abecasis, G., Durbin, R., and Genome Project Data Processing, S. (2009). The sequence alignment/map format and SAMtools. Bioinformatics *25*, 2078–2079.

Love, M.I., Huber, W., and Anders, S. (2014). Moderated estimation of fold change and dispersion for RNA-seq data with DESeq2. Genome Biol. *15*, 550.

Lynch, M.R., and Tang, J. (2020). COVID-19 and kidney injury. Rhode Isl. Med. J. *103*, 24–28.

Malakauskas, S., Quan, H., Fields, T., McCall, S., Yu, M., Kourany, W., Frey, C., and Le, T. (2007). Aminoaciduria and altered renal expression of luminal amino acid transporters in mice lacking novel gene collectrin. Am. J. Physiol. Renal. Physiol. *292*, F533–F544.

Mizuiri, S., Hemmi, H., Arita, M., Aoki, T., Ohashi, Y., Miyagi, M., Sakai, K., Shibuya, K., Hase, H., and Aikawa, A. (2011). Increased ACE and decreased ACE2 expression in kidneys from patients with IgA nephropathy. Nephron Clin. Pract. *117*, c57–66.

Mizuiri, S., Hemmi, H., Arita, M., Ohashi, Y., Tanaka, Y., Miyagi, M., Sakai, K., Ishikawa, Y., Shibuya, K., Hase, H., et al. (2008). Expression of ACE and ACE2 in individuals with diabetic kidney disease and healthy controls. Am. J. Kidney Dis. *51*, 613–623.

Mizuiri, S., and Ohashi, Y. (2015). ACE and ACE2 in kidney disease. World J. Nephrol. *4*, 74–82.

Mokhtari, T., Hassani, F., Ghaffari, N., Ebrahimi, B., Yarahmadi, A., and Hassanzadeh, G. (2020). COVID-19 and multiorgan failure: a narrative review on potential mechanisms. J. Mol. Histol. *51*, 613–628.

Moon, J.Y., Jeong, K.H., Lee, S.H., Lee, T.W., Ihm, C.G., and Lim, S.J. (2008). Renal ACE and ACE2 expression in early diabetic rats. Nephron Exp. Nephrol. *110*, e8–e16.

Mount, D. (2007). Collectrin and the kidney. Curr. Opin. Nephrol. Hypertens. *16*, 427–429.

Ng, K.W., Attig, J., Bolland, W., Young, G.R., Major, J., Wrobel, A.G., Gamblin, S., Wack, A., and Kassiotis, G. (2020). Tissue-specific and interferon-inducible expression of nonfunctional ACE2 through endogenous retroelement co-option. Nat. Genet. *52*, 1294–1302.

Onabajo, O.O., Banday, A.R., Stanifer, M.L., Yan, W., Obajemu, A., Santer, D.M., Florez-Vargas, O., Piontkivska, H., Vargas, J.M., Ring, T.J., et al. (2020). Interferons and viruses induce a novel truncated ACE2 isoform and not the full-length SARS-CoV-2 receptor. Nat. Genet. *52*, 1283–1293.

Park, M., Kwon, C.H., Ha, H.K., Han, M., and Song, S.H. (2020). RNA-Seq identifies condition-specific biological signatures of ischemia-reperfusion injury in the human kidney. BMC Nephrol. *21*, 398.

Peng, L., Liu, J., Xu, W., Luo, Q., Chen, D., Lei, Z., Huang, Z., Li, X., Deng, K., Lin, B., et al. (2020). SARS-CoV-2 can be detected in urine, blood, anal swabs, and oropharyngeal swabs specimens. J. Med. Virol. *92*, 1676–1680.

Renteria, A., Mfuna Endam, L., Adam, D., Filali-Mouhim, A., Maniakas, A., Rousseau, S., Brochiero, E., Gallo, S., and Desrosiers, M. (2020). Azithromycin downregulates gene expression of IL-1β and pathways involving TMPRSS2 and TMPRSS11D required by SARS-CoV-2. Am. J. Respir. Cell. Mol. Biol. *63*, 707–709.

Risso, D., Ngai, J., Speed, T.P., and Dudoit, S. (2014). Normalization of RNA-seq data using factor analysis of control genes or samples. Nat. Biotechnol. *32*, 896–902.

Su, H., Yang, M., Wan, C., Yi, L.X., Tang, F., Zhu, H.Y., Yi, F., Yang, H.C., Fogo, A.B., Nie, X., et al. (2020). Renal histopathological analysis of 26 postmortem findings of patients with COVID-19 in China. Kidney Int. *98*, 219–227.

Sun, J., Zhu, A., Li, H., Zheng, K., Zhuang, Z., Chen, Z., Shi, Y., Zhang, Z., Chen, S.B., Liu, X., et al. (2020). Isolation of infectious SARS-CoV-2 from urine of a COVID-19 patient. Emerg. Microbes Infect *9*, 991–993.

Sungnak, W., Huang, N., Becavin, C., Berg, M., Queen, R., Litvinukova, M., Talavera-Lopez, C., Maatz, H., Reichart, D., Sampaziotis, F., et al. (2020). SARS-CoV-2 entry factors are highly expressed in nasal epithelial cells together with innate immune genes. Nat. Med. *26*, 681–687.

Thorvaldsdottir, H., Robinson, J.T., and Mesirov, J.P. (2013). Integrative Genomics Viewer (IGV): high-performance genomics data visualization and exploration. Brief Bioinform *14*, 178–192.

Thurman, R.E., Rynes, E., Humbert, R., Vierstra, J., Maurano, M.T., Haugen, E., Sheffield, N.C., Stergachis, A.B., Wang, H., Vernot, B., et al. (2012). The accessible chromatin landscape of the human genome. Nature *489*, 75–82.

Tipnis, S.R., Hooper, N.M., Hyde, R., Karran, E., Christie, G., and Turner, A.J. (2000). A human homolog of angiotensin-converting enzyme. Cloning and functional expression as a captopril-insensitive carboxypeptidase. J. Biol. Chem. *275*, 33238–33243.

Vinayagam, S., and Sattu, K. (2020). SARS-CoV-2 and coagulation disorders in different organs. Life Sci. *260*, 118431.

Wang, Y., John, R., Chen, J., Richardson, J., Shelton, J., Bennett, M., Zhou, X., Nagami, G., Zhang, Y., Wu, Q., et al. (2009). IRF-1 promotes inflammation early after ischemic acute kidney injury. J. Am. Soc. Nephrol. *20*, 1544–1555.

Wang, G., Kwan, B.C., Lai, F.M., Choi, P.C., Chow, K.M., Li, P.K., and Szeto, C.C. (2010). Intrarenal expression of miRNAs in patients with hypertensive nephrosclerosis. Am. J. Hypertens. *23*, 78–84.

Wu, H., Chen, G., Wyburn, K., Yin, J., Bertolino, P., Eris, J., Alexander, S., Sharland, A., and Chadban, S. (2007). TLR4 activation mediates kidney ischemia/reperfusion injury. J. Clin. Invest. *117*, 2847–2859.

Zhang, M., Wang, X., Wang, Y., Niu, A., Wang, S., Zou, C., and Harris, R. (2017). IL-4/IL-13-mediated polarization of renal macrophages/dendritic cells to an M2a phenotype is essential for recovery from acute kidney injury. Kidney Int. *91*, 357–386.

Ziegler, C.G.K., Allon, S.J., Nyquist, S.K., Mbano, I.M., Miao, V.N., Tzouanas, C.N., Cao, Y., Yousif, A.S., Bals, J., Hauser, B.M., et al. (2020). SARS-CoV-2 receptor ACE2 is an interferon-stimulated gene in human airway epithelial cells and is detected in specific cell subsets across tissues. Cell *181*, 1016–1035.e9.

STAR★METHODS

KEY RESOURCES TABLE

REAGENT or RESOURCE	SOURCE	IDENTIFIER
Antibodies		
Anti-Trimethyl-Histone H3 (Lys4)	Millipore	Cat# 07-473; RRID:AB_1977252
Anti-RNA polymerase II CTD repeat	Abcam	Cat# ab5408; RRID:AB_304868
Anti-Histone H3K27ac	Active Motif	Cat# 39133; RRID:AB_2561016
Anti-Histone H3K4me1	Active Motif	Cat# 39297; RRID:AB_2615075
Chemicals, peptides, and recombinant proteins		
Human IFNα	Stem Cell Tech.	Cat# 78077
Human IFNβ	Peprotech	Cat# 300-02BC
Human IFNγ	Peprotech	Cat# 300-02
Human IL-1β	Peprotech	Cat# 200-01B
Human TNFα	Peprotech	Cat# 300-01A
Human IL-6	Peprotech	Cat# 200-06
Ruxolitinib	Peprotech	Cat# 9414958
Critical commercial assays		
SsoAdvanced Universal Probes Supermix	Bio-rad	Cat# 172-5281
PureLink RNA Mini Kit	Invitrogen	Cat# 12183018A
SuperScript III First-Strand Synthesis SuperMix	Invitrogen	Cat# 18080-400
NEBNext® Ultra™ II DNA Library Prep Kit	New England Bio.	Cat# E7645L
TruSeq total RNA Library Prep Kit	Illumina	Cat# 20020597
Deposited data		
Original ChIP-seq data – cytokine-stimulated human proximal tubule cells	NCBI GEO data set	GSE161915
Original RNA-seq data – cytokine-stimulated human proximal tubule cells	NCBI GEO data set	GSE161916
RNA-seq – human AKI kidney	NCBI GEO data set	GSE142077
RNA-seq – human COVID-19 kidney	NCBI GEO data set	GSE150316
RNA-seq – lung epithelium + IFNβ	NCBI GEO data set	GSE161665
RNA-seq – liver epithelium + IFNβ	NCBI GEO data set	GSE115198
CTCF ChIP-seq - HEK293	NCBI GEO data set	GSE68976
DHS - Human Renal Cortical Epithelial cells	NCBI GEO data set	GSE29692
Hi-C - human adrenal gland	Northwestern University Yue Lab database	http://3dgenome.fsm.northwestern.edu/view.php
Human reference genome NCBI build 37, GRCh37	Genome Reference Consortium	http://www.ncbi.nlm.nih.gov/projects/genome/assembly/grc/human/
Experimental models: Cell lines		
Human Primary Proximal Tubule (HPPT) Cells	ATCC	Cat# PCS-400-010
Oligonucleotides		
Human *GAPDH* Taqman probe mix	Thermo Fisher	Hs02786624_g1
Human *ACE2* Taqman probe mix	Thermo Fisher	Hs01085333_m1
Human *TMPRSS2* Taqman probe mix	Thermo Fisher	Hs01122322_m1
Human *STAT1* Taqman probe mix	Thermo Fisher	Hs01013996_m1
Custom *dACE2* qRT-PCR probe	Eurofins Genomics	N/A

(*Continued on next page*)

Continued

REAGENT or RESOURCE	SOURCE	IDENTIFIER
Custom full-length *ACE2* qRT-PCR probe	Eurofins Genomics	N/A
Custom dACE2 PCR primers	Eurofins Genomics	N/A
Custom ACE2 PCR primers	Eurofins Genomics	N/A
Software and algorithms		
Trimmomatic (version 0.36)	Bolger et al., 2014	http://www.usadellab.org/cms/?page=trimmomatic
Bowtie (version 1.1.2)	Langmead et al., 2009	http://bowtie-bio.sourceforge.net/manual.shtml
Integrative Genomics Viewer	Thorvaldsdóttir et al., 2013	http://software.broadinstitute.org/software/igv/
STAR (2.5.4a)	Dobin et al., 2013	https://anaconda.org/bioconda/star/files?version=2.5.4a
HTSeq	Anders et al., 2015	https://htseq.readthedocs.io/en/master/
Bioconductor	Huber et al., 2015	https://www.bioconductor.org/
RUVSeq	Risso et al., 2014	https://bioconductor.org/packages/release/bioc/html/RUVSeq.html
DESeq2	Love et al., 2014	https://bioconductor.org/packages/release/bioc/html/DESeq2.html
Samtools	Li et al., 2009	http://www.htslib.org/
PRISM GraphPad (8.4.3)	GraphPad Software	https://www.graphpad.com/scientific-software/prism/

RESOURCE AVAILABILITY

Lead contact

Further information and requests for resources and reagents should be directed to and will be fulfilled by the Lead Contact, Lothar Hennighausen (lotharh@nih.gov).

Materials availability

This study did not generate new unique reagents.

Data and code availability

The original RNA-seq and ChIP-seq data from HPPT cells were submitted to the Gene Expression Omnibus under GEO: GSE161917 (ChIP-seq - GEO: GSE161915, RNA-seq - GEO: GSE161916), and are publicly available. Accession numbers are also listed in the key resources table. Additional supplemental items are available from Mendeley Data: https://doi.org/10.17632/zhvggb5b44.1. DHS from human renal cortical epithelial cells and CTCF ChIP-seq from HEK293 cells were obtained under GEO: GSE29692 and GEO: GSE68976, respectively. RNA-seq data for IFNβ-stimulated lung and liver cell were obtained from GEO: GSE161665 and GEO: GSE115198, respectively. Human AKI and COVID-19 data were found under GEO: GSE142077 and GEO: GSE150316, respectively. Hi-C data from human adrenal gland tissues were obtained from Hi-C data browser (http://3dgenome.fsm.northwestern.edu/view.php).

Any additional information required to reanalyze the data reported in this paper is available from the lead contact upon request.

EXPERIMENTAL MODEL AND SUBJECT DETAILS

Cell culture

HPPT cells (ATCC® PCS-400-010™) from a male donor were cultured in low-serum medium consisting of Renal Epithelial Cell Basal Medium (ATCC® PCS-400-030™) with Renal Epithelial Cell Growth Kit (ATCC® PCS-400-040™), Penicillin-Streptomycin-Amphotericin B Solution (ATCC® PCS-999-002™), and Phenol red (ATCC® PCS-999-001™) added. Cells were obtained at passage 2, cultured according to the manufacturer's instructions, and used between passages 4 and 6. In addition to characteristic cobblestone growth pattern when confluent, cells were confirmed to express several proximal tubule markers including γ-glutamyltransferase-1 and *SLC3a1* as assessed with RNA-seq (Lee et al., 2015).

METHOD DETAILS

Cytokine stimulation

Cells were stimulated with IFNα (Stem Cell Technologies), IFNβ, IFNγ, TNFα, IL-6, and IL-1β (all obtained from Peprotech) for 12 hours in concentration of 10 ng/ml. Cells were treated with ruxolitinib (Peprotech) at 10 μM for 12 hours together with IFNβ. At least three biological replicates were prepared for all experiments.

RNA isolation and qRT-PCR

After cytokine stimulation, cells were washed twice with phosphate buffered saline (PBS) before RNA isolation to remove medium and debris. mRNA was isolated using PureLink™ RNA Mini Kit (Invitrogen), and 500 ng was transcribed into cDNA using SuperScript™ III First-Strand Synthesis SuperMix (Invitrogen). qRT-PCR reaction was prepared with SsoAdvanced Universal Probes Supermix (Bio-Rad) and the following Taqman probes (ThermoFisher): *GAPDH* (Hs02786624_g1), *ACE2* (Hs01085333_m1), *TMPRSS2* (Hs01122322_m1), and *STAT1* (Hs01013996_m1) or the following primers: *dACE2* forward: 5′ GGAAGCAG GCTGGGACAAA 3′, *dACE2* reverse: 5′ AGCTGTCAGGAAGTCGTCCATT 3′, ACE2 forward: 5′ GGGCGAC TTCAGGATCCTTAT 3′, ACE2 reverse: 5′ GGATATGCCCCATCTCATGATG 3′. Custom qRT-PCR probe sequences were as follows: *ACE2*: 5′ [6~FAM] ATGGACGACTTCCTGACAG [MGBE~Q] 3′, *dACE2*: 5′ [6~FAM] AGGGAGGATCCTTATGTG [MGBE~Q] 3′. Reaction conditions were as follows: initial denaturation for 3 minutes at 95°C and 40 cycles of 10 seconds at 95°C and 30 seconds at 60°C.

PCR amplification

ACE2 PCR was performed with cDNA obtained as described earlier. Fifty nanograms of cDNA was used in the following reaction: initial denaturation – 3 minutes, 98°C and 35 cycles of denaturation – 30 seconds at 98°C, annealing – 30 seconds at 58°C, extension – 72°C for 2 minutes, ending with final extension of 72°C for 10 minutes. Amplified fragments were run on a 1.5% agarose in 1x TAE gel with 100-kb DNA ladder to assess product size. Bands were cut out, and PCR products cleaned with MinElute Gel Extraction Kit (Quiagen) and Sanger sequenced by Quintara Biosciences. Primers used were as follows: dACE2 forward: 5′-TGTGAGAGCCTTAGGTTGGATTCC-3′, dACE2 reverse: 5′-TCTCTCCTTGGCCATGTTGT-3′ (Onabajo et al., 2020).

RNA-seq library preparation and data analysis

mRNA was prepared as described earlier and quality assessed using Bioanalyzer 2100 (Agilent). Samples with adequate RIN values were transcribed into libraries using TruSeq total RNA Library Prep Kit according to the manufacturer's instructions. Libraries were pooled in equimolar amounts and sequenced using HiSeq 2000 (Illumina).

The raw data were subjected to QC analyses using the FastQC tool (version 0.11.9) (https://www.bioinformatics.babraham.ac.uk/projects/fastqc/). Trimmomatic (version 0.36) (Bolger et al., 2014) was used to assess total RNA-seq read quality, and STAR RNA-seq (version 2.5.4a) (Dobin et al., 2013) using 50-bp paired-end mode was used to align the reads (hg19). HTSeq (Anders et al., 2015) was used to retrieve the raw counts, and R package DESeq2 (Huber et al., 2015; Love et al., 2014) was used to normalize data. Additionally, the RUVSeq (Risso et al., 2014) package was applied to remove confounding factors. A minimum of five reads was an additional basis for filtering artifacts. The visualization was done using dplyr (https://CRAN.R-project.org/package=dplyr) and ggplot2 (Risso et al., 2014). Significantly differential expressed genes with an adjusted p-value (pAdj, FDR) below 0.05 and a fold change > 2 for upregulated genes were categorized using GSEA (https://www.gsea-msigdb.org/gsea/msigdb). Sequence read numbers were calculated using Samtools (Li et al., 2009) software with sorted bam files.

ChIP-seq library preparation and data analysis

Cells were washed twice with PBS and fixed with 0.75% formaldehyde in Dulbecco's Modified Eagle Medium (DMEM) for 10 minutes in room temperature. Next, glycine was added to quench fixation in a final concentration of 125 mM, and plates were incubated in room temperature for another 10 minutes. Cells were then scraped and centrifuged at 4°C, for 1 minute, at 3000 rpm, and then washed twice with cold PBS. Pellets were resuspended in 2 ml of Farnham Lysis Buffer with protease inhibitors and incubated on ice for 10 minutes. Then, the cells were pelleted again at 4°C, for 5 minutes, at 3500 rpm and resuspended in TE buffer with protease inhibitors. Chromatin was sonicated for 3 minutes using a probe sonicator

(Active Motif). Finally, after centrifugation at 4°C, 13000 g for 10 minutes, the supernatant was used for immunoprecipitation.

Briefly, 600-1000 μg of chromatin was incubated with antibody-coated Dynabeads™ Protein A (Invitrogen) at 4°C overnight. The beads were then washed with radioimmunoprecipitation assay buffer (RIPA), high-NaCl RIPA, LiCl buffer, and PBS. Next, DNA was eluted from the beads and reverse cross-linked by incubating with proteinase K at 65°C overnight. DNA was then purified with MinElute PCR Purification Kit (Quiagen), and library preparation was performed according to the manufacturer's instructions for NEBNext® Ultra™ II DNA Library Prep Kit for Illumina® (New England Biotechnology). Proper library size distribution with a peak in 300- to 500-bp range was confirmed using Bioanalyzer 2100 (Aligent), libraries pooled and sequenced with HiSeq 2000 (Illumina). Antibodies used were as follows: anti-Trimethyl-Histone H3 (Lys4) (Millipore, 07-473), Anti-RNA polymerase II CTD repeat (Abcam, ab5408), Anti-Histone H3K27ac (Active Motif, 39133), Anti-Histone H3K4me1 (Active Motif, 39297)

Quality filtering and alignment of the raw reads was performed using Trimmomatic (Bolger et al., 2014) (version 0.36) and Bowtie (Langmead et al., 2009) (version 1.1.2), with the parameter '-m 1' to keep only uniquely mapped reads, using the reference genome hg19. Picard tools (Broad Institute, Picard, http://broadinstitute.github.io/picard/. 2016) was used to remove duplicates and subsequently, and Homer (Heinz et al., 2010) (version 4.8.2) software was applied to generate bedGraph files. Integrative Genomics Viewer (Thorvaldsdottir et al., 2013) was used for visualization.

QUANTIFICATION AND STATISTICAL ANALYSIS

Statistical analysis of data was performed using Prism 8. First, normal distribution of data was assessed. Next, statistical significance was evaluated with 1-way or 2-way AVOVA followed by Tukey's multiple comparisons, or a T-test, depending on the experimental setup. n and points on a graph always represent biological replicates – seeded wells of a 6-well culture plate. Values of *$p < 0.05$, **$p < 0.01$, ***$p < 0.001$, ****$p < 0.0001$ were considered statistically significant.